

## Discrete structure in the 3*d* photoabsorption spectra of neutral, singly ionized and doubly ionized bromine

Anthony Cummings and Gerry O'Sullivan

*Physics Department, University College Dublin, Belfield, Dublin 4, Ireland*

(Received 20 November 1995)

The 3*d* photoabsorption spectra of Br, Br<sup>+</sup>, and Br<sup>2+</sup> have been recorded photographically in the 60–90 eV region using the dual-laser-produced plasma technique. In each case intense 3*d*→4*p* transitions were observed while 3*d*→*np* (*n*>4) features were also obtained in the spectrum of neutral bromine. The transitions were classified with the aid of multiconfiguration Hartree-Fock calculations. The excited states are predicted to decay by direct autoionization involving 4*s* or 4*p* electrons and the rates for the different processes and resulting linewidths were also calculated. From these data theoretical cross sections for the observed features were also computed. [S1050-2947(96)01507-7]

PACS number(s): 32.80.Hd, 32.30.Jc, 52.50.Jm

### I. INTRODUCTION

In a recent paper the usefulness of the dual-laser-produced plasma (DLP) method for the investigation of inner-shell photoabsorption of chalcogen and halogen atoms and ions was discussed and specifically demonstrated in the case of 4*d* shell photoabsorption of I, I<sup>+</sup>, and I<sup>2+</sup> [1]. The reactive and transient nature of such atoms has severely limited experimental investigation in the past. Previous studies with the DLP method have been restricted largely to metals and the targets used were pure single element samples; see, e.g., [2–4]. However, if a suitable composite or salt target is selected it is possible to obtain photoabsorption spectra of the constituent elements. In the present case we report on the discrete structure obtained near the bromine 3*d* threshold using compressed pellets of KBr and CsBr as targets.

The ground state of neutral bromine is 3*d*<sup>10</sup>4*s*<sup>2</sup>4*p*<sup>5</sup> <sup>2</sup>P<sub>3/2</sub> and valence shell excitation by electric-dipole-allowed processes gives rise to 4*p*→*ns,nd* Rydberg series converging on the <sup>3</sup>P<sub>2</sub>, <sup>3</sup>P<sub>1</sub>, <sup>3</sup>P<sub>0</sub>, <sup>1</sup>D<sub>2</sub>, and <sup>1</sup>S<sub>0</sub> states of Br<sup>+</sup>. Early studies on emission spectra established a number of series converging on the <sup>2</sup>P states [5]. Subsequent absorption studies on microwave or flash pyrolysis dissociated Br<sub>2</sub> identified further series and enabled the energies of the <sup>1</sup>D<sub>2</sub> and <sup>1</sup>S<sub>0</sub> states to be derived [6–8]. Photoelectron spectra produced by irradiation with unpolarized HeI-α 584 Å radiation have also been reported [9,10] and the latter work also included measurements of relative differential cross sections for the 4*p*<sup>-1</sup> ionic state. Theoretical 4*p*<sup>-1</sup> photoionization cross sections have also been calculated within the Hartree-Fock approximation and compared with valence photoexcitation of other halogens [11], while a subsequent *R*-matrix calculation for the total photoionization below the <sup>1</sup>S<sub>0</sub> threshold reproduced the essential features of the autoionising structure [12]. For 4*s*<sup>-1</sup> excitation, although the 4*s*<sup>2</sup>4*p*<sup>5</sup> <sup>2</sup>P<sub>3/2</sub>→4*s*4*p*<sup>6</sup> <sup>2</sup>S<sub>1/2</sub> transition was observed in very early spectroscopic studies [5], 4*s*→*np* (*n*≥5) transitions have only been reported very recently [13]. Angle-resolved photoelectron spectroscopy was used to investigate the photoexcitation of a microwave dissociated Br<sub>2</sub> beam by synchrotron radiation. Energies and effective quantum numbers for

4*s*<sup>2</sup>4*p*<sup>5</sup> <sup>2</sup>P<sub>3/2</sub>→4*s*4*p*<sup>5</sup>*np* (<sup>2</sup>P, <sup>2</sup>D) features up to *n*=10 were reported and compared with the analogous 4*s*<sup>2</sup>4*p*<sup>6</sup> <sup>1</sup>S<sub>0</sub>→4*s*4*p*<sup>6</sup>*np* <sup>1</sup>P series in Kr. It was found that the quantum defects were almost identical in both cases and that

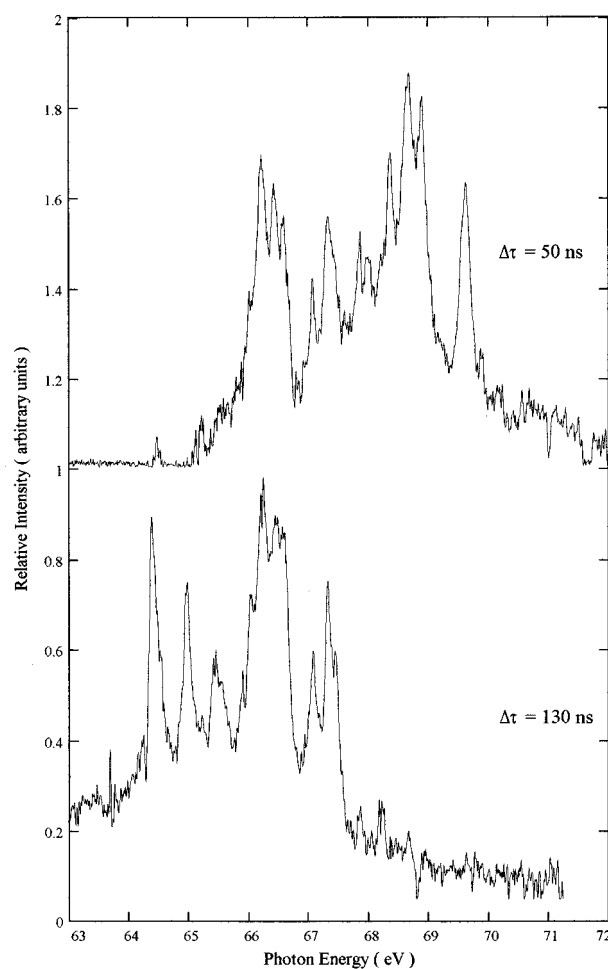


FIG. 1. Densitometer traces of absorption spectra from a laser-produced plasma containing bromine obtained with radiation from a samarium plasma as the backlighter recorded at different time delays. The absorbing path lengths were 12 mm in each case.

TABLE I. Theoretical and observed energies,  $gf$  values, and autoionization widths of the most intense  $3d \rightarrow np$  ( $n \geq 5$ ) transitions of neutral bromine.

Transition	$E_{\text{HF}}+0.80$ (eV)	$10^3 gf$	$\Gamma$ (meV)	$E$ (eV) <sup>a</sup>	$E$ (eV) <sup>b</sup>
${}^2P_{3/2} \rightarrow 5p({}^1D) {}^2P_{3/2}$	75.29	7	75.4	75.35	75.39
$\rightarrow 5p({}^1D) {}^2P_{1/2}$	75.31	5	75.3		
$\rightarrow 5p({}^3D) {}^2P_{3/2}$	75.42	21	111.1		
$\rightarrow 5p({}^3D) {}^2D_{5/2}$	75.46	15	104.8		
${}^2P_{1/2} \rightarrow 5p({}^3D) {}^4D_{3/2}$	75.63	14	94.7	75.60	75.56
${}^2P_{3/2} \rightarrow 5p({}^3F) {}^2D_{5/2}$	75.66	35	76.5		
${}^2P_{1/2} \rightarrow 5p({}^2D) {}^2P_{1/2}$	75.76	17	95.5	75.90	75.83
$\rightarrow 5p({}^3F) {}^4D_{3/2}$	75.86	31	81.6		
${}^2P_{3/2} \rightarrow 5p({}^3D) {}^4P_{1/2}$	76.14	5	85.4	76.30	76.22
${}^2P_{1/2} \rightarrow 5p({}^3P) {}^4D_{1/2}$	76.14	14	70.6		
${}^2P_{3/2} \rightarrow 5p({}^3D) {}^4P_{3/2}$	76.16	6	96.6		
$\rightarrow 5p({}^3F) {}^4D_{5/2}$	76.27	6	76.8	76.30	76.22
$\rightarrow 5p({}^3F) {}^4F_{5/2}$	76.35	7	77.5		
${}^2P_{1/2} \rightarrow 5p({}^3F) {}^4D_{3/2}$	76.59	38	78.6	76.70	76.58
${}^2P_{3/2} \rightarrow 6p({}^1D) {}^2P_{3/2}$	76.60	4	74.9		
$5p({}^3P) {}^4P_{3/2}$	76.61	5	73.0		
$5p({}^3P) {}^2D_{5/2}$	76.67	5	73.2	76.70	76.70
${}^2P_{1/2} \rightarrow 5p({}^3F) {}^4F_{3/2}$	76.70	24	75.9		
${}^2P_{3/2} \rightarrow 6p({}^3D) {}^2P_{3/2}$	76.72	9	111.0	76.85	76.85
$\rightarrow 5p({}^3P) {}^2S_{1/2}$	76.73	11	75.3		
${}^2P_{1/2} \rightarrow 5p({}^3P) {}^4D_{3/2}$	76.76	11	71.3		
${}^2P_{3/2} \rightarrow 6p({}^3F) {}^2D_{5/2}$	76.93	29	72.2	76.85	76.85
$\rightarrow 5p({}^1F) {}^2D_{5/2}$	77.06	7	89.4		
${}^2P_{1/2} \rightarrow 6p({}^3F) {}^4D_{3/2}$	77.20	21	76.5	77.15	77.16
${}^2P_{3/2} \rightarrow 7p({}^3F) {}^2D_{5/2}$	77.40	7	71.4	77.40	74.40
${}^2P_{1/2} \rightarrow 5p({}^1P) {}^2S_{1/2}$	77.42	18	43.8	77.55	77.50
${}^2P_{3/2} \rightarrow 8p({}^3F) {}^2D_{5/2}$	77.67	10	71.7	77.95	78.40
${}^2P_{1/2} \rightarrow 6p({}^3F) {}^4F_{3/2}$	78.01	20	73.6		
$\rightarrow 7p({}^3F) {}^4F_{3/2}$	78.49	11	71.4	78.40	

<sup>a</sup>Measured approximately from Fig. 2 of Ref. [17].

<sup>b</sup>Present work.

the series formed window resonances. In addition, a number of doubly excited  $4s^2 4p^5 \rightarrow 4s^2 4p^3 n l n' l'$  resonances were also detected and absolute partial photoionization cross sections and asymmetry parameters for  $4p$  photoionization both in the resonance regions and at selected energies between the  $4p^{-1}$  and  $4s^{-1}$  thresholds were evaluated. The results at nonresonant energies were in good agreement with the earlier Hartree-Fock (HF) calculations [11]. Subsequently the eigenchannel  $R$ -matrix method was used to determine partial and differential cross sections below the  $4s 4p^5$  threshold [14] and again reproduced the essential details of the  $4s^{-1}$  resonances and measured partial cross sections, any differences being attributable to the fact the calculation did not specifically include double valence excitation.

The earliest reported study of  $3d$  photoabsorption identified three resonances measured at 64.38, 65.43, and 64.97 eV as  $3d^{10} 4s^2 4p^5 \rightarrow 3d^9 4s^2 4p^2 {}^2P_{3/2} \rightarrow {}^2D_{5/2}$ ,  ${}^2P_{3/2} \rightarrow {}^2D_{3/2}$ , and  ${}^2P_{1/2} \rightarrow {}^2D_{3/2}$  transitions [15]. Photoelectron spectroscopy (PES) on a laser photodissociated Br gas jet backlit by monochromatized synchrotron radiation gave positions of

64.54, 65.58, and 65.3 for these features and autoionization widths of 100 and 90 meV for the  $3d^{-1} {}^2D_{5/2}$  and  ${}^2D_{3/2}$  states, respectively [16]. Furthermore, a detailed theoretical study of the relaxation dynamics of these states concluded that direct autoionization into  $3d^{10} 4s^2 4p^4$ ,  $3d^{10} 4s 4p^5$ , and  $3d^{10} 4p^6$  were the dominant decay mechanisms.

In the decay to the  $3d^{10} 4s^2 4p^4$  configuration preferential population of the  ${}^1D$  and  ${}^1S$  states rather than  ${}^3P$  was predicted by theory and confirmed experimentally. For decay to  $3d^{10} 4s 4p^5$  strong mixing between  $4s 4p^5 ({}^1P)$ ,  $4s^2 4p^3 ({}^2P) 4d^1 P$ , and  $4s^2 4p^3 ({}^2D) 4d^1 P$  had to be invoked to account for the structure observed in the PES spectrum where ten well-resolved peaks were obtained. Subsequently, features due to  $3d \rightarrow np$  ( $n > 4$ ) excitation recorded using the same technique as  $3d \rightarrow 4p$  were reported [17]. The spectrum was found to contain two well-resolved peaks below the  $3d^{-1} {}^2D_{5/2}$  threshold and at least five other features that together spanned the energy range from 75 to 79 eV. No attempt was made to classify these spectra, but from a comparison with similar  $4d \rightarrow np$  ( $n \geq 5$ ) features in iodine it was

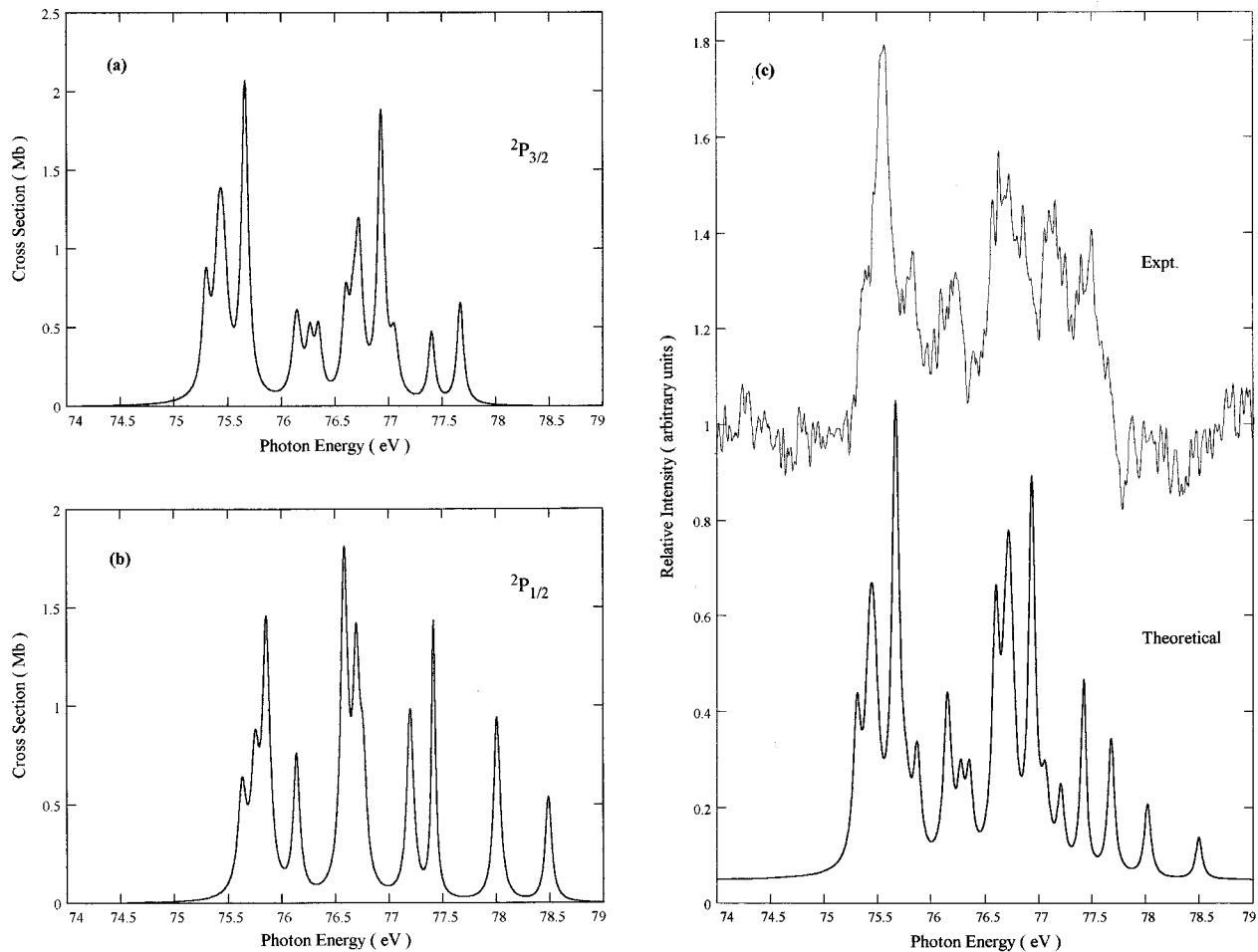


FIG. 2. Predicted cross sections for  $3d \rightarrow np$  ( $n > 4$ ) photoabsorption in neutral bromine from both (a) ground ( $^2P_{3/2}$ ) and (b) excited state ( $^2P_{1/2}$ ) terms. (c) Comparison between theory and experiment. Note that the relative contributions were assumed to be 70%  $^2P_{3/2}$  and 30%  $^2P_{1/2}$ .

concluded that the excited states decayed preferentially by a resonant Auger process. In the present paper we again report an observation of the  $3d \rightarrow np$  ( $n > 4$ ) spectra recorded with improved resolution and an attempt is made to classify the strongest features, using the Cowan suite of atomic structure codes [18]. We also report the observation of the  $3d$  photoabsorption spectra of  $\text{Br}^+$  and  $\text{Br}^{2+}$ . To the authors' knowledge, subvalence photoabsorption spectra of these ions have not been reported previously because of the difficulties of preparing an ionized beam of sufficient density. In addition to energy levels, oscillator strengths and linewidths are also calculated and from these absolute photoionization cross sections are deduced. These data are important for future investigations using synchrotron radiation crossed with ion beams and indeed can only be verified using such techniques as the methods used here at best give only relative cross-section information.

## II. EXPERIMENT

The experimental system has already been described elsewhere [1–3]. A 1-J, 30-ns  $Q$ -switched ruby laser pulse was focused onto a KBr or CsBr target (which had been com-

pressed at high pressure to form a pellet) to yield a plasma column containing ionized bromine. Focusing was achieved with a crossed cylindrical lens assembly, which gives a plasma whose width is 200  $\mu\text{m}$  and whose length can be varied between 2 and 12 mm. The backlighting continuum was produced by tightly focusing an 860-mJ, 10-ns Nd:YAG pulse (where YAG denotes yttrium aluminum garnet) onto a Sm or Yb target. Variation of the interlaser pulse delay  $\Delta\tau$  or laser pulse power density  $\Phi$  on the target makes it possible to obtain spectra in which different ion stages are optimized or at least occur in very different ratios. The spectra were recorded on a 2-m grazing incidence spectrograph with a 1200-g/mm grating and an entrance slit width of 20  $\mu\text{m}$ . Under these conditions the instrumental resolving power is 0.005 eV in the energy region of interest. It was found that for  $\Delta\tau \leq 50$  ns the spectrum consisted of a mixture of  $\text{Br}^+$  and  $\text{Br}^{2+}$ , for  $\Delta\tau \sim 130$  ns it was predominantly  $\text{Br}^+$ , while for  $\Delta\tau > 500$  ns neutral Br predominated. The spectra were calibrated by superimposing emission lines from an aluminium plasma [19]. Measurements were performed with a photoelectric comparator and digital densitometer. The measurement accuracy is estimated as  $\pm 0.03$  eV and is limited by the inherent width of the features.

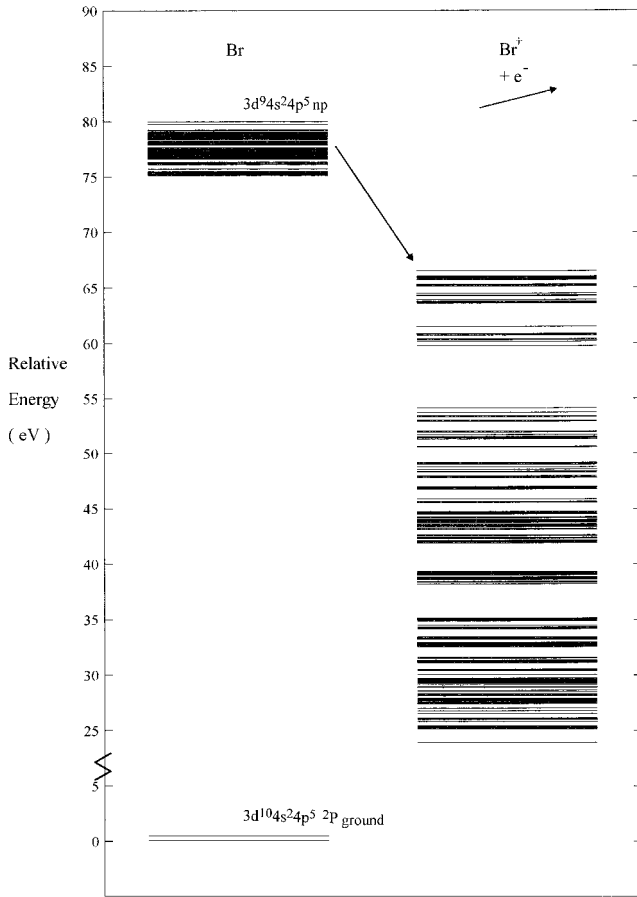


FIG. 3. Excitation and decay pathways used to determine the energies and widths of the  $3d \rightarrow np$  ( $n > 4$ ) features in the spectrum of neutral bromine.

### III. RESULTS

#### A. Neutral bromine

A spectrum obtained at a time delay  $\Delta\tau$  of 130 ns and an absorption path length of 12 mm corresponding to an average flux on target of  $10^{13} \text{ W m}^{-2}$  is presented in Fig. 1. It contains lines of Br and  $\text{Br}^+$ . The features with peak intensities at 64.38, 64.97, and 65.43 eV correspond to the  $3d^{10}4s^24p^5 \rightarrow 3d^94s^24p^6 \ ^2P_{3/2} \rightarrow ^2D_{5/2}$ ,  $^2P_{1/2} \rightarrow ^2D_{3/2}$ , and  $^2P_{3/2} \rightarrow ^2D_{3/2}$  of neutral bromine. These measurements agree with the earlier values of Mazzoni and Pettini [15] rather than the later data of [16]. *Ab initio* calculations with the Cowan RCN, RCN2, and RCG suite of codes [18] predict that the  $^2P_{3/2} \rightarrow ^2D_{5/2}$  to  $^2P_{3/2} \rightarrow ^2D_{3/2}$  intensity ratio should be 8.46 and this agrees with observations [16]. In the spectrum of Fig. 1 the observed ratio is approximately 2, which indicates either plate saturation or a nonlinear photographic response or both. The intensity of the  $^2P_{1/2} \rightarrow ^2D_{3/2}$  transition indicates that a sizable population exists in the  $^2P_{1/2}$  metastable state. The measured widths of the  $^2D_{5/2}$  and  $^2D_{3/2}$  levels are 100 and 90 meV, respectively [16]. Autoionization calculations in which the  $F^k(nl;nl)$  integrals were reduced by 10% while all other Slater Condon parameters were left unchanged were also performed with the Cowan code. If decay to  $3d^{10}4s^24p^4$ ,  $3d^{10}4s4p^5$ , and  $3d^{10}4p^6$  configura-

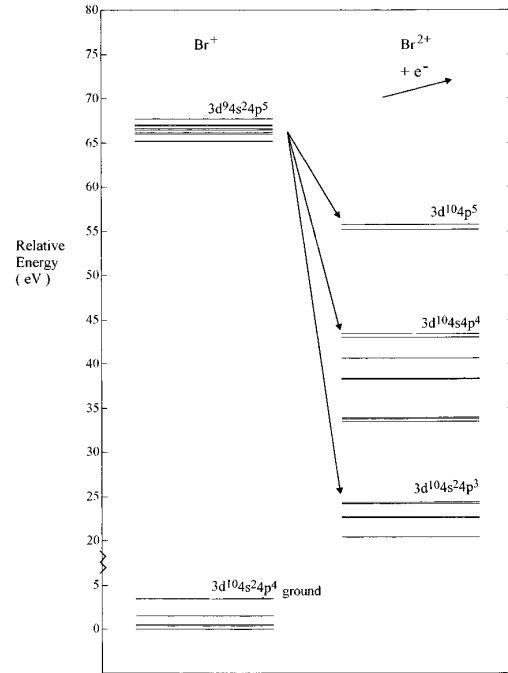


FIG. 4. Excitation and decay pathways used to determine  $3d \rightarrow 4p$  excitation energies and decay widths in the spectrum of  $\text{Br}^+$ . Note that the ground and  $3d^94s^24p^5$  energies correspond to observed and/or fitted values while the energies of the final states reached in the decay process are *ab initio* calculated values.

tions are allowed for, the predicted linewidths are 95 meV in each case. Reduction of  $F^k$ ,  $G^k$ , or  $R^k$  integrals leads to a further reduction in linewidth. Since the agreement with experiment is reasonably good a similar scaling of parameters was used in all subsequent calculations for each ion stage. If the line profile is assumed to be Lorentzian, which indeed appears to be the case here, then the cross section  $\sigma$  can be written (in Mb) as  $\sigma = 109.7 f_k / 2\pi [(E_k - E)^2 + \Gamma_k^2/4]$ , where  $E_k$  and  $\Gamma_k$  are the energy and linewidth of the transition (in eV) and  $f_k$  is the oscillator strength. Hence it was possible to calculate the cross section for the observed features. The values obtained were 45.5 and 5.4 Mb for  $^2P_{3/2} \rightarrow ^2D_{5/2}$  and  $^2D_{3/2}$ , respectively, and 54.3 Mb for  $^2P_{1/2} \rightarrow ^2D_{3/2}$ .

As already pointed out, a photoabsorption spectrum containing a number of discrete features arising from  $3d \rightarrow np$  ( $n \geq 5$ ) transitions has been reported by Nahon and Morin [17]. We have also observed these features and calculated their energies, oscillator strengths, and linewidths using  $3d^94s^2[4p^6 + 4p^5(5p + 6p + 7p + 8p)]$  as an excited-state basis. Transitions to  $nf$  states were not included as the presence of a large centrifugal barrier in the  $l=3$  potential expels these states from the core region and they have negligible oscillator strength as a consequence [20]. Although these calculations predict almost 400 lines, as with iodine [1], consideration of only the strongest transitions, i.e., those with  $gf > 0.001$ , successfully reproduces the spectrum. The results of these calculations are summarized in Table I and shown graphically in Figs. 2(a) and 2(b), where all transitions are included regardless of  $gf$  value. They are compared with the experimental spectrum in Fig. 2(c), where the  $^2P_{3/2}$  and  $^2P_{1/2}$

TABLE II. Theoretical and observed energies,  $gf$  values, and autoionization widths of the  $3d^{10}4d^24p^4 \rightarrow 3d^94s^24p^5$  transition array in  $\text{Br}^+$ .

Transition	$E_{\text{calc}}$ (eV)	$10^3 gf$	$\Gamma$ (meV)	$E_{\text{obs}}$ (eV)	$I^a$
$^1S_0 \rightarrow ^3D_1$	63.46	17	86.7		
$\rightarrow ^3P_1$	64.03	13	75.1		
$^1D_2 \rightarrow ^1D_2$	64.52	66	74.6	64.48	$10^b$
$\rightarrow ^3D_3$	64.64	3	110.0		
$^1S_0 \rightarrow ^1P_1$	65.18	116	42.7	65.21	10
$^1D_2 \rightarrow ^3D_2$	65.40	12	101.5		
$\rightarrow ^3D_1$	65.41	1	86.7		
$\rightarrow ^3F_3$	65.53	49	75.0	65.52	$10^b$
$^3P_1 \rightarrow ^1D_2$	65.63	17	74.6	65.59	$10^b$
$^1D_2 \rightarrow ^3P_2$	65.89	20	70.6		
$\rightarrow ^3P_1$	65.99	0	75.1		
$^3P_2 \rightarrow ^1D_2$	66.02	58	74.6	66.0	60
$\rightarrow ^3D_3$	66.13	47	110.0	66.21	100
$^1D_2 \rightarrow ^3F_2$	66.32	14	71.2		
$\rightarrow ^1F_3$	66.41	569	110.3	66.45	80
$^3P_0 \rightarrow ^3D_1$	66.43	129	86.7		
$^3P_1 \rightarrow ^3D_2$	66.50	269	101.5	66.52	70
$\rightarrow ^3D_1$	66.52	31	86.7		
$^3P_2 \rightarrow ^3D_2$	66.89	19	101.5		
$\rightarrow ^3D_1$	66.91	1	86.7		
$^3P_1 \rightarrow ^3P_2$	67.00	11	70.6		
$^3P_0 \rightarrow ^3P_1$	67.01	0	75.1		
$^3P_0 \rightarrow ^3P_1$	67.01	0	75.0		
$^3P_1 \rightarrow ^3P_1$	67.10	82	75.1	67.07	30
$^1D_2 \rightarrow ^1P_1$	67.14	7	42.7		
$^3P_2 \rightarrow ^3P_2$	67.39	137	70.6	67.30	60
$^3P_1 \rightarrow ^3F_2$	67.43	0	71.2		
$^3P_2 \rightarrow ^3P_1$	67.49	46	75.1	67.44	40
$^3P_1 \rightarrow ^3P_0$	67.51	138	69.1		
$^3P_2 \rightarrow ^3F_2$	67.82	9	71.2	67.86	10
$\rightarrow ^1F_3$	67.91	0	110.3		
$^3P_0 \rightarrow ^1P_1$	68.16	20	42.7	68.19	15
$^3P_1 \rightarrow ^1P_1$	68.25	0	42.7		
$^3P_2 \rightarrow ^1P_1$	68.34	6	42.7	68.66	5

<sup>a</sup>Visual estimates.

<sup>b</sup>Blended with lines of neutral bromine.

populations are weighted as 70% and 30%, respectively. Agreement between the theoretical and experimental spectra is optimized if the former is shifted by 0.8 eV towards higher energy. Because of this close agreement and the good correlation between observed and calculated intensities it was possible to assign all of the observed features. These classifications are listed in Table I together with experimental energies. The energies of the features observed by Nahon and Morin, determined approximately from Fig. 2 of their paper, are also included for comparison. Most of the features correspond to blends of a number of the stronger transitions. An interesting fact is that the features noted by Nahon and Morin at 77.95 and 78.40 eV are absent from our data. According to the calculations these features originate from  $^2P_{1/2}$  photoexcitation from which it must be concluded that these

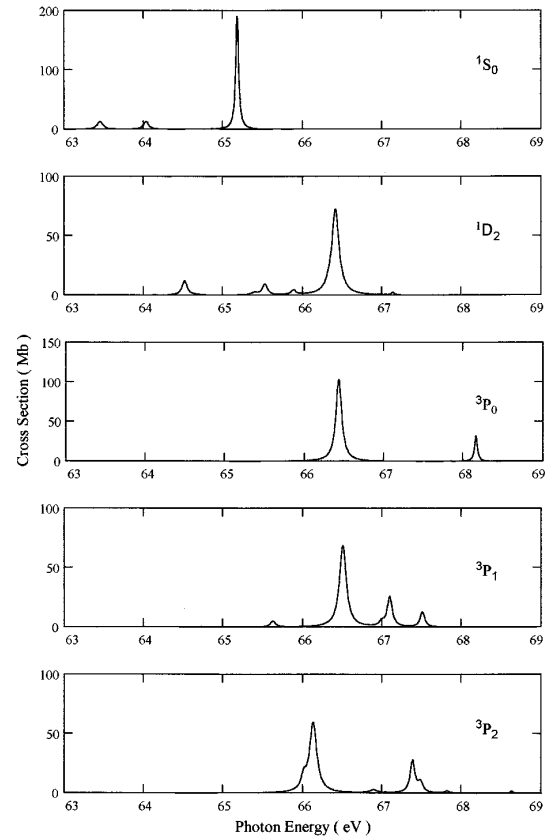


FIG. 5. Theoretical cross sections for  $3d \rightarrow 4p$  photoabsorption for each term of the  $3d^{10}4s^24p^4$  configuration of  $\text{Br}^+$ .

authors had an appreciable population of excited bromine in their atomic beam. The remaining strong feature due to  $^2P_{1/2}$  excitation at 75.90 eV is evident in both spectra.

Also listed in Table I are autoionizing linewidths for each of the excited terms. In performing these calculations the configuration average energies ( $E_{\text{av}}$ ) of  $3d^{10}4s^24p^4$ ,  $3d^{10}4s^24p^34d$ ,  $3d^{10}4s4p^5$ ,  $3d^{10}4s^24p^35p$ ,  $3d^{10}4s^24p^24d5p$ ,  $3d^{10}4s4p^45p$ ,  $3d^{10}4p^6$ , and  $3d^{10}4p^55p$  were first obtained. The kinetic energy of the electron ejected in the decay of each  $3d^94s^24p^4np$  term was evaluated with respect to each of these and used to specify the energies of the continuum  $\epsilon l$  electrons. In similar calculations for iodine it was noted that if final-state term energies were chosen instead of  $E_{\text{av}}$  and the partial linewidths for decay to each of these were evaluated and summed, the final value differed from that obtained using  $E_{\text{av}}$  directly by at most only a few percent [1]. A diagram showing the calculated term energies of all possible final states is presented in Fig. 3. Note that all energies are relative to the  $^2P_{3/2}$  energy. We expect the calculated linewidths to be quite reliable considering the accuracy of the  $3d \rightarrow 4p$  predictions and the fact that earlier calculations by McGuire indicated linewidths of 90 meV for  $3d^{-1}np$  hole states [21]. From the calculations it is apparent that decay to  $3d^{10}4s^24p^35p$ ,  $3d^{10}4s4p^45p$ , and  $3d^{10}4p^55p$  are the dominant channels for the  $3d^{-1}5p$  state. For higher  $np$  states the probability of shake-off processes where both a valence and the Rydberg electron are ejected simultaneously is expected to be enhanced and cause an increase in line-

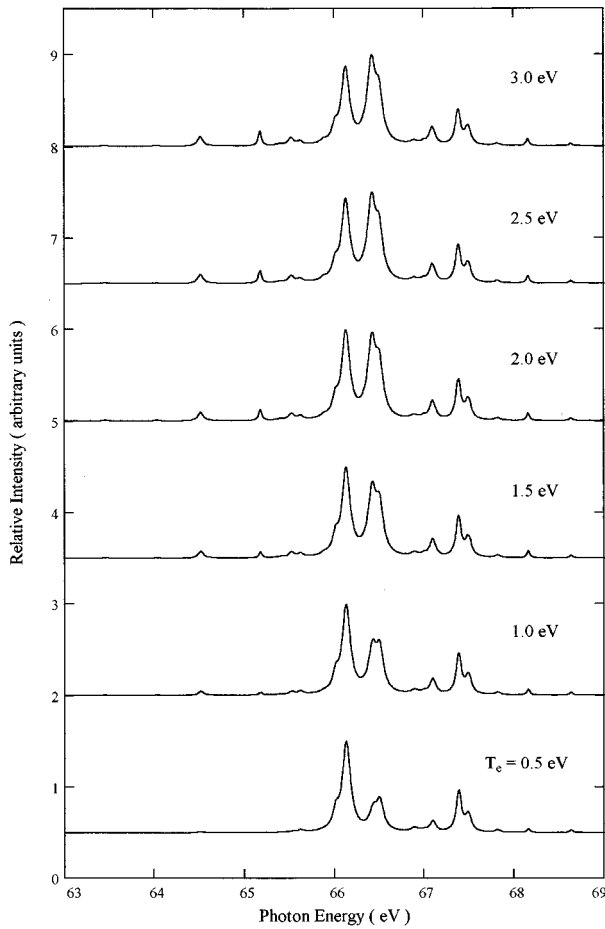


FIG. 6. Changes in the theoretical  $\text{Br}^+$   $3d \rightarrow 4p$  absorption profile due to differing excited-state populations consistent with electron temperatures in the range 0.5–3.0 eV.

width. In the case of the adjacent element Kr ( $Z=36$ ), for example, it was found that  $3d^{-1}np$  states decayed preferentially into  $\text{Kr}^{2+} + 2e^-$  [12]. From an investigation of resonance Auger spectra it was concluded that the  $3d^9 5p$  decays primarily by two-step autoionization. In the first step the decay proceeds to  $4s^{-1}$  or  $4p^{-1}$  states with the  $5p$  remaining as a spectator or being shaken up to an  $n'p$  state [22]. The excitation then subsequently decays to the  $4p^{-2}$  configuration of  $\text{Kr}^{2+}$  [23]. For higher Rydberg states the linewidth due to resonant Auger processes should decrease with  $n$  [24], but experimentally is found to be approximately constant, pointing to the increased importance of shake-off processes at higher energy [25]. Combet-Farnoux [26] has investigated the decay of the homologous  $4d^9 5s^2 5p^5 np$  states of iodine in considerable detail. The situation here is more complicated because of the large multiplet splitting within the  $4d^9 5s^2 5p^5$  parent configuration. She concluded that direct autoionization in which the Rydberg electron acts as a spectator or is involved in a shake-up process is the most important route for decay to  $4d^{10} 5s^2 5p^3 6p$ , while decay to  $4d^{10} 5s 5p^4 6p$  can be followed by further ionization in which the  $6p$  electron can participate. Strong mixing of  $5s 5p^4 6p + 5s^2 5p^2 5d 6p$  leads to a whole range of double ionization thresholds  $5s 5p^4 + 5s^2 5p^2 5d$  in addition to

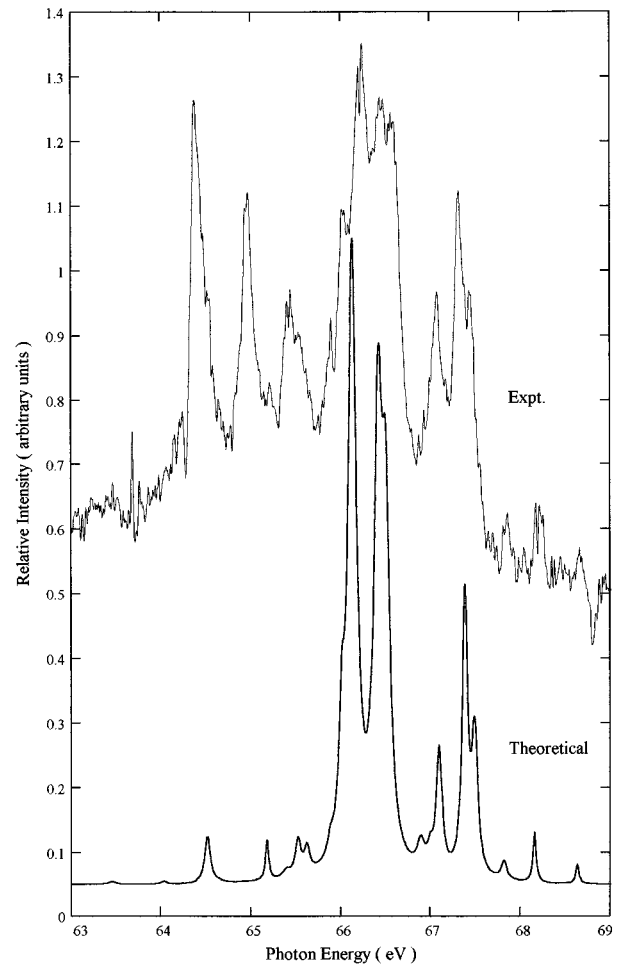


FIG. 7. Comparison between the observed and the calculated  $\text{Br}^+$  spectrum for an electron temperature of 1.5 eV.

$5s^2 5p^3$ , which need to be accounted for in linewidth calculations and to explain the Auger spectra. These predictions were subsequently verified [17]. Combet-Farnoux further postulated that shake-off rather than spectator or shake-up processes must be considered as soon as  $n$  is high enough to involve higher  $n'd$  states in the configuration mixing  $5s 5p^4 np + 5s^2 5p^2 n' dnp$ . In the present case we anticipate that an identical situation will prevail, especially as we have seen that theory indicates that direct decay to  $4s^{-1}$  or  $4p^{-1}$  completely dominates over  $5p$  shake-off in the first autoionization step.

### B. Singly ionized bromine

The ground state of  $\text{Br}^+$  is  $3d^{10} 4s^2 4p^4 \ ^3P_2$  and the positions of the excited  $^3P_1$ ,  $^3P_0$ ,  $^1D_2$ , and  $^1S_0$  states have been established previously [6]. In Fig. 1, a number of features arising from  $3d^{10} 4s^2 4p^4 \rightarrow 3d^9 4s^2 4p^5$  transitions in  $\text{Br}^+$  are evident between 64 and 69 eV. As before, calculations were performed for  $3d^{10} 4s^2 4p^4 \rightarrow 3d^9 4s^2 [4p^5 + 4p^4(5p + 7p + 8p)]$  and transition energies,  $gf$  values, and linewidths evaluated. For the latter partial linewidths for the decay pathways,  $3d^9 4s^2 4p^5 \rightarrow 3d^{10} 4s^2 4p^3 + \epsilon l$ ,  $3d^{10} 4s 4p^4 + \epsilon l$ , and  $3d^{10} 4p^5 + \epsilon l$  were evaluated and

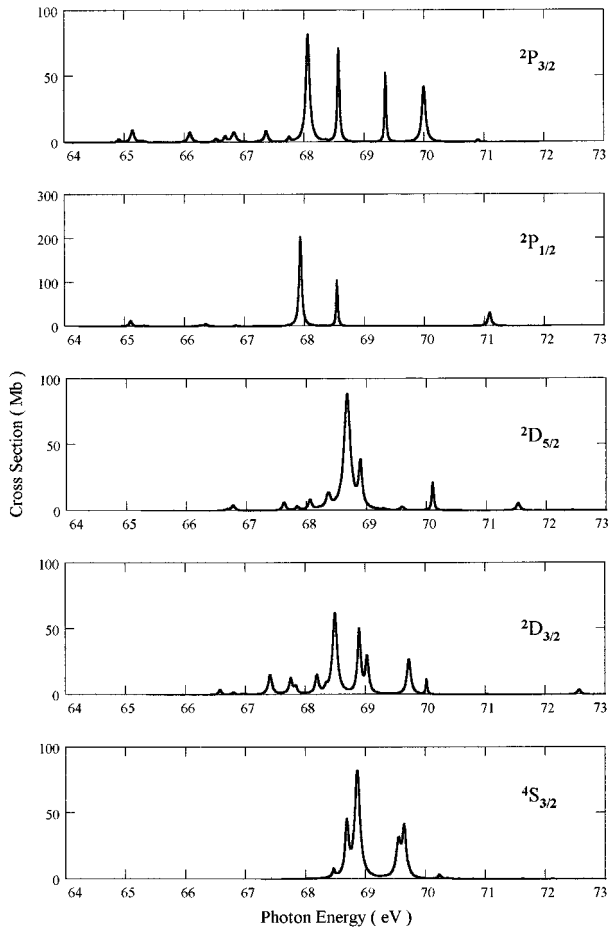


FIG. 8. Theoretical cross sections for  $3d \rightarrow 4p$  photoabsorption for each term of the  $3d^{10}4s^24p^3$  configuration of  $\text{Br}^{2+}$ .

summed. The term energy diagram for all processes considered is given in Fig. 4. From these data theoretical cross sections for excitation from each of the  $3d^{10}4s^24p^4$  terms were computed. From comparison between experimental and theoretical data it was possible to assign all of the observed peaks.

The detailed classifications are presented in Table II. A particular feature here is the agreement between the observed energy  $E_{\text{obs}}$  and the calculated energy  $E_{\text{calc}}$ . It should be noted that  $E_{\text{calc}}$  is not the energy calculated directly from the HF codes, but was obtained as follows: first the  $3d^94s^24p^5$  energies were calculated relative to  $E_{\text{av}}$  of the  $3d^{10}4s^24p^4$  configuration; then using known values for the term energies of the  $3d^{10}4s^24p^4$  the true value of  $E_{\text{av}}$  was estimated and the  $3d^94s^24p^5$  terms shifted to compensate for the difference between actual and theoretical values. The difference between individual term energies using HF values for the upper configuration and observed values for the lower one were then taken to yield the energy of each possible transition and a constant energy shift of 0.626 eV determined by least-squares fitting of the observed to the calculated peaks was added to each value. As before, there is an excellent correlation between oscillator strength and observed intensities, especially when the nonlinearity of the spectral recording is remembered. Also it should be noted that absorption

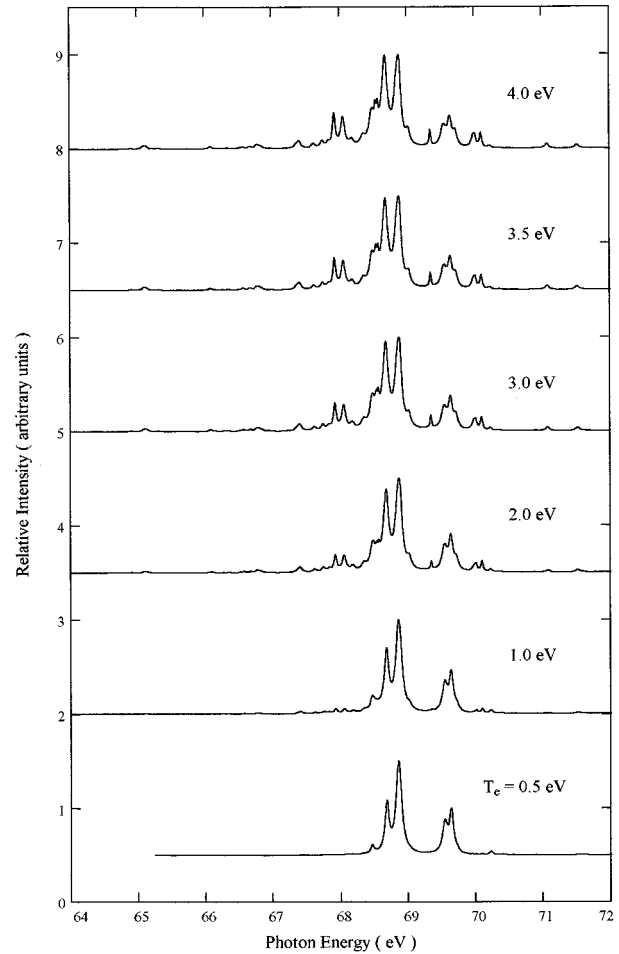


FIG. 9. Changes in the theoretical  $\text{Br}^{2+}$   $3d \rightarrow 4p$  absorption profile due to differing excited-state populations consistent with electron temperatures in the range 0.5–4.0 eV.

from excited terms of the ground configuration clearly contribute to the spectrum. It is of interest to compare the calculated and observed spectra in order to make a quantitative estimate of the importance of excited state absorption. In Fig. 5 the photoabsorption cross section for each term of the  $3d^{10}4s^24p^4$  configuration is presented. Here the theoretical energies correspond to  $E_{\text{calc}}$ . The corresponding absorption for different thermal populations at plasma electron temperatures ranging from 0.5 to 3.0 eV are shown in Fig. 6. From the comparison of these data with observation it is seen that the relative contributions expected for a plasma electron temperature in the range 1.5–2.0 eV fit the experimental data quite well, especially when the nonlinearity of plate response at low light levels is allowed for (Fig. 7). Finally, term energies and eigenvectors in  $LS$  coupling are presented in Table III. It should be noted that the average purity in the  $LS$  scheme was 80% for the  $3d^94s^24p^5$  configuration compared to 72% for the  $jj$  scheme, so the former was chosen to label the terms.

At higher energies, between 82.4 and 85 eV, some weaker structure due to  $3d \rightarrow 5p$  excitation was also observed. It was not possible to make any detailed assignments as hundreds of

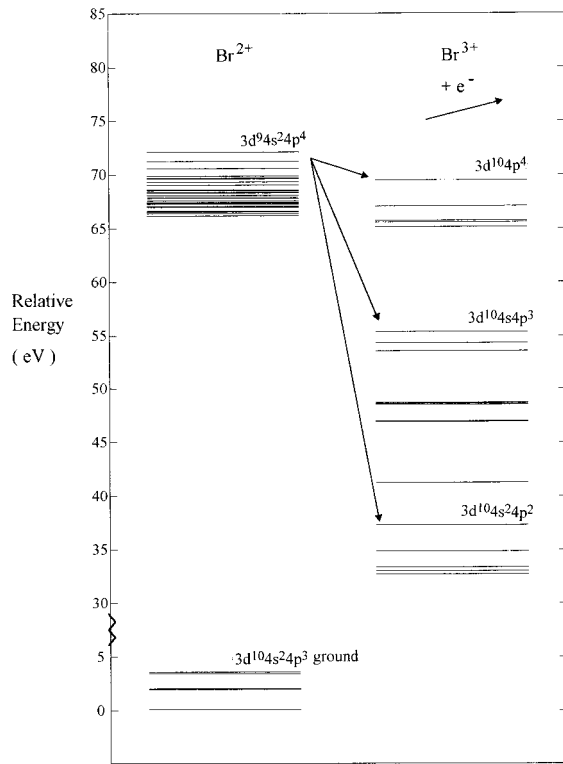


FIG. 10. Excitation and decay pathways for  $3d \rightarrow 4p$  photoexcitation in  $\text{Br}^{2+}$ . As before, the  $3d^{10}4s^2 4p^3$  state energies are experimental values, the  $3d^9 4s^2 4p^4$  energies are experimental or fitted values, while energies of the final states reached in the decay process are *ab initio* theoretical values.

TABLE III. Term energies and eigenvector composition of the  $3d^{10}4s^2 4p^4$  and  $3d^9 4s^2 4p^5$  configurations of  $\text{Br}^+$ .

Configuration	$J$	Term	$E_{\text{obs}}$ (eV)	% $LS$
$3d^{10}4s^2 4p^4$	0	$^1S$	3.455 <sup>a</sup>	98% $^1S$
		$^3P$	0.476 <sup>a</sup>	98% $^3P$
	1	$^3P$	0.389 <sup>a</sup>	100% $^3P$
	2	$^3P$	0	98% $^3P$
		$^1D$	1.499 <sup>a</sup>	98% $^1D$
	$3d^9 4s^2 4p^5$	0	$^3P$	67.83
$^1P$			68.67	68% $^1P$ - 25% $^3P$ + 7% $^3D$
$^3P$			67.44	64% $^3P$ + 27% $^3D$ + 10% $^1P$
2		$^3D$	66.91	67% $^3D$ - 20% $^1P$ - 12% $^3P$
		$^3P$	67.30	80% $^3P$ + 10% $^3F$ - 7% $^1D$
		$^1D$	65.99	76% $^1D$ + 14% $^3D$ + 6% $^3P$
3		$^3D$	66.93	81% $^3D$ - 10% $^3P$ - 8% $^1D$
		$^3F$	67.86	84% $^3F$ + 10% $^1D$ - 5% $^3P$
		$^3D$	66.21	96% $^3D$
		$^1F$	67.95	88% $^1F$ - 9% $^3F$
		$^3F$	67.02	90% $^3F$ + 9% $^1F$

<sup>a</sup>Energies from Ref. [6].

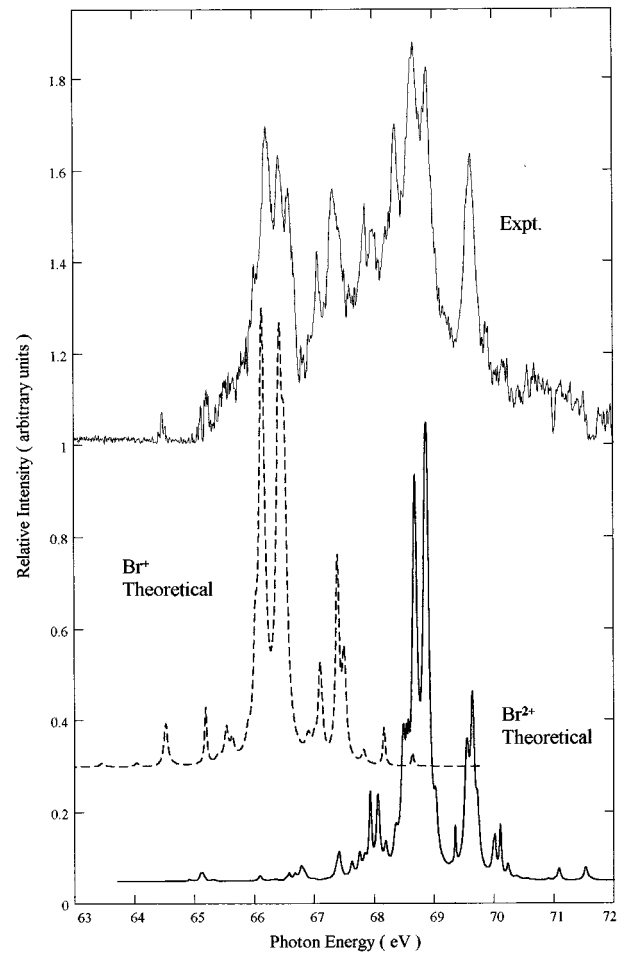


FIG. 11. Comparison between the observed and the calculated  $\text{Br}^{2+}$  spectrum for an electron temperature of 2.0 eV. The calculated  $\text{Br}^+$  spectrum for the same electron temperature is also included. The differences in peak heights between predicted and observed spectra can be attributed to the fact that for large absorption the photographic response is almost logarithmic and can also suffer from reciprocity failure.

lines blend to form a near-continuum-like structure throughout this energy range.

### C. Doubly ionized bromine

In Fig. 1 the spectrum obtained for an interlaser delay of 50 ns and an absorbing path length of 12 mm is also presented. In addition to the features identified as  $\text{Br}^+$  lines it contains discrete structure at higher energies that arises from  $3d^{10}4s^2 4p^3 \rightarrow 3d^9 4s^2 4p^4$  excitation in  $\text{Br}^{2+}$ . The ground term of this ion is  $^4S_{3/2}$ , while the  $^2D_{3/2}$ ,  $^2D_{5/2}$ ,  $^2P_{1/2}$ , and  $^2P_{3/2}$  levels are known from vacuum spark emission spectra to lie 1.89, 2.02, 3.37, and 3.553 eV higher in energy [27]. As before, by consideration of  $3d^{10}4s^2 4p^3 \rightarrow 3d^9 4s^2 [4p^4 + 4p^3(5p + 6p + 7p + 8p)]$  excitation, transition energies, oscillator strengths, and autoionizing linewidths were calculated and used to generate an absorption cross section for each state of the lowest configuration (Fig. 8), while the changes in overall profile due to excited-state absorption are presented in Fig. 9 for plasma electron tem-

TABLE IV. Theoretical and observed energies,  $gf$  values, and autoionization widths of the most intense ( $gf > 0.01$ ) lines of the  $3d^{10}4s^24p^3 \rightarrow 3d^94s^24p^4$  array in  $\text{Br}^{2+}$ .

Transition	$E_{\text{calc}}$ (eV)	$10^3 gf$	$\Gamma$ (meV)	$E_{\text{obs}}$ (eV)	$I^*$
$^2P_{1/2} \rightarrow (^3P) ^2P_{1/2}$	65.09	19	49.5		
$^2P_{3/2} \rightarrow (^3P) ^2P_{3/2}$	65.13	36	67.9		
$\rightarrow (^3P) ^4P_{3/2}$	66.09	20	73.9		
$\rightarrow (^3P) ^4D_{5/2}$	66.09	10	57.6		
$^2P_{1/2} \rightarrow (^3P) ^4F_{3/2}$	66.35	10	65.7		
$^2P_{3/2} \rightarrow (^3P) ^2F_{5/2}$	66.52	10	67.2		
$^2D_{3/2} \rightarrow (^3P) ^2P_{1/2}$	66.57	12	49.5		
$^2P_{3/2} \rightarrow (^3P) ^4D_{3/2}$	66.68	15	55.1		
$^2D_{5/2} \rightarrow (^3P) ^4F_{7/2}$	66.78	26	72.0		
$^2P_{3/2} \rightarrow (^1D) ^2D_{5/2}$	66.83	38	88.6		
$^2P_{3/2} \rightarrow (^3P) ^2D_{5/2}$	67.36	64	65.9		
$^2D_{3/2} \rightarrow (^3P) ^4F_{5/2}$	67.41	33	74.6		
$^2D_{5/2} \rightarrow (^3P) ^4P_{3/2}$	67.62	11	73.9		
$\rightarrow (^3P) ^4D_{5/2}$	67.62	22	57.6	67.60	10
$^2D_{3/2} \rightarrow (^3P) ^4P_{3/2}$	67.75	11	73.9		
$\rightarrow (^3P) ^4D_{5/2}$	67.75	30	57.6		
$^2P_{3/2} \rightarrow (^3P) ^2D_{3/2}$	67.75	10	50.1		
$^2D_{3/2} \rightarrow (^3P) ^4F_{3/2}$	67.83	21	65.7		
$^2D_{5/2} \rightarrow (^3P) ^4D_{7/2}$	67.85	15	61.0		
$^2P_{1/2} \rightarrow (^3P) ^2D_{3/2}$	67.93	292	50.1	67.86	20
$^2D_{5/2} \rightarrow (^3P) ^2F_{5/2}$	68.05	43	67.2		
$^2P_{3/2} \rightarrow (^1D) ^2F_{5/2}$	68.06	338	71.5	68.00	20
$^2D_{3/2} \rightarrow (^3P) ^2F_{3/2}$	68.18	52	67.2		
$\rightarrow (^3P) ^4D_{3/2}$	68.34	12	55.1		
$^2D_{5/2} \rightarrow (^1D) ^2D_{5/2}$	68.36	81	88.6		
$^2S_{3/2} \rightarrow (^3P) ^2P_{1/2}$	68.46	17	49.5		
$^2D_{3/2} \rightarrow (^1P) ^2D_{5/2}$	68.49	315	88.6	68.36	60
$^2P_{1/2} \rightarrow (^1D) ^2P_{1/2}$	68.53	84	28.4		
$^2P_{3/2} \rightarrow (^1D) ^2P_{3/2}$	68.57	159	39.0		
$^2D_{5/2} \rightarrow (^1D) ^2F_{7/2}$	68.68	918	121.8		
$^4S_{3/2} \rightarrow (^3P) ^2P_{3/2}$	68.68	155	67.9	68.67	100
$^4S_{3/2} \rightarrow (^3P) ^4P_{5/2}$	68.86	469	101.0	68.90	80
$^2D_{3/2} \rightarrow (^1D) ^2D_{3/2}$	68.89	175	63.3		
$^2D_{5/2} \rightarrow (^3P) ^2D_{5/2}$	68.89	188	65.9		
$^2D_{3/2} \rightarrow (^3P) ^2D_{5/2}$	69.02	116	65.9		
$^2P_{3/2} \rightarrow (^1D) ^2S_{1/2}$	69.35	88	28.7		
$^4S_{3/2} \rightarrow (^3P) ^4P_{1/2}$	69.54	142	92.1		
$^2D_{5/2} \rightarrow (^3P) ^2D_{5/2}$	69.59	16	71.5	69.63	80
$^4S_{3/2} \rightarrow (^3P) ^4P_{3/2}$	69.64	148	73.9		
$^2D_{3/2} \rightarrow (^3P) ^2D_{5/2}$	69.72	116	71.5		
$^2P_{3/2} \rightarrow (^1S) ^2D_{5/2}$	69.99	172	70.5	69.87	10
$^2D_{3/2} \rightarrow (^1D) ^2P_{1/2}$	70.01	18	28.4		
$^2D_{5/2} \rightarrow (^1D) ^2P_{3/2}$	70.10	71	39.0		
$^4S_{3/2} \rightarrow (^3P) ^4D_{3/2}$	70.23	10	55.1	70.18	10
$^2P_{1/2} \rightarrow (^1S) ^2D_{3/2}$	71.08	55	61.7		
$^2D_{5/2} \rightarrow (^1S) ^2D_{5/2}$	71.52	34	70.5		
$^2D_{3/2} \rightarrow (^1S) ^2D_{3/2}$	72.56	14	61.7		

TABLE V. Term energies and eigenvector compositions of the  $3d^{10}4s^24p^3$  and  $3d^94s^24p^4$  configurations of  $\text{Br}^{2+}$ .

Configuration	$J$	Term	$E_{\text{obs}}$ (eV)	% $LS$
$3d^{10}4s^24p^3$	1/2	$^2P$	3.370 <sup>a</sup>	100% $^2P^a$
	3/2	$^4S$	0	98% $^4S^a$
		$^2P$	3.553 <sup>a</sup>	91% $^2P+7\% ^2D^a$
		$^2D$	1.890 <sup>a</sup>	92% $^2D+8\% ^2P^a$
	5/2	$^2D$	2.021 <sup>a</sup>	100% $^2D^a$
$3d^94s^24p^4$	1/2	$(^3P) ^2P$		84% $(^3P) ^2P+9\% (^3P) ^4P$
		$(^3P) ^4P$	69.63	90% $(^3P) ^4P-7\% (^3P) ^2P$
		$(^3P) ^4D$	70.18	93% $(^3P) ^4D+6\% (^3P) ^2P$
		$(^1D) ^2P$		63% $(^1D) ^2P-34\% (^1D) ^2S$
		$(^1D) ^2S$		65% $(^1D) ^2S+34\% (^1D) ^2P$
	3/2	$(^3P) ^2P$	68.67	53% $(^3P) ^2P+43\% (^3P) ^4P$
		$(^3P) ^4P$	69.63	50% $(^3P) ^4P-29\% (^3P) ^2P+9\% (^3P) ^4F+7\% (^3P) ^4D$
		$(^3P) ^4F$		66% $(^3P) ^4F-12\% (^3P) ^4D-12\% (^3P) ^2D$
		$(^3P) ^4D$		66% $(^3P) ^4D+14\% (^3P) ^4F+8\% (^3P) ^2D+8\% (^3P) ^2P$
		$(^1D) ^2D$	70.79	49% $(^1D) ^2D-18\% (^3P) ^2D-14\% (^1D) ^2P-8\% (^3P) ^4F+6\% (^3P) ^4D$
		$(^3P) ^2D$	71.23	59% $(^3P) ^2D+22\% (^1D) ^2D-7\% (^3P) ^4D-6\% (^1D) ^2P$
		$(^1D) ^2P$		77% $(^1D) ^2P+17\% (^1D) ^2D$
		$(^1S) ^2D$		90% $(^1S) ^2D+8\% (^1D) ^2D$
	5/2	$(^3P) ^4F$		65% $(^3P) ^4F+28\% (^3P) ^2F$
		$(^3P) ^4F$	69.62	65% $(^3P) ^4D+12\% (^3P) ^2F+10\% (^3P) ^2D-9\% (^3P) ^4F$
		$(^3P) ^2F$		44% $(^3P) ^2F-24\% (^3P) ^4D-18\% (^3P) ^4F+7\% (^1D) ^2F-6\% (^1D) ^2D$
		$(^1D) ^2D$	70.25	61% $(^1D) ^2D-18\% (^1D) ^2F+7\% (^3P) ^2F-7\% (^1S) ^2D$
		$(^1D) ^2F$	71.55	36% $(^1D) ^2F+37\% (^3P) ^2D+16\% (^1D) ^2D-6\% (^3P) ^2F$
		$(^1S) ^2D$		87% $(^1S) ^2D+9\% (^1D) ^2D$
	7/2	$(^3P) ^4P$		49% $(^3P) ^4F+25\% (^3P) ^2F+12\% (^1D) ^2F+14\% (^3P) ^4D$
$(^3P) ^4D$			48% $(^3P) ^4D-41\% (^3P) ^4F+5\% (^1D) ^2F$	
$(^3P) ^2F$			-29% $(^3P) ^2F+38\% (^3P) ^4D$	
			-22% $(^1D) ^2F+9\% (^3P) ^4F+9\% (^3P) ^4F$	
$(^1D) ^2F$		70.69	58% $(^1D) ^2F-41\% (^3P) ^2F$	
	$(^1D) ^2G$		96% $(^1D) ^2G$	

<sup>a</sup>Energies and eigenvectors from Ref. [27].

peratures ranging from 0.5 to 4.0 eV. The results of these calculations are summarized in Table IV. The excited-state lifetimes were calculated by allowing for the decay channels

$$\begin{aligned}
3d^94s^24p^4 &\rightarrow 3d^{10}4s^24p^2\epsilon l \quad (l=0,2,4) \\
&\rightarrow 3d^{10}4s4p^3\epsilon l \quad (l=1,3) \\
&\rightarrow 3d^{10}4p^4\epsilon l \quad (l=0,2,4),
\end{aligned}$$

and their detailed term structure is shown in Fig. 10. Interestingly, the contribution of  $3d^94s^24p^4 \rightarrow 3d^{10}4s4p^24d\epsilon l$  to the autoionizing linewidth is predicted to be negligible as observed in the homologous  $4d^95s^25p^4 \rightarrow 4d^{10}5s5p^25d\epsilon l$  of  $\text{I}^{2+}$  [1]. In Fig. 11(a) direct comparison is made between theoretical and experimental results. The individual contribu-

tions of the different levels of the ground configuration were summed in the ratio corresponding to a 2.0-eV plasma, which is seen to reproduce the experimental data quite well. The classifications made on the basis of this comparison are also included in Table IV. In Table V the term energies derived from the assignments of Table IV are listed along with eigenvector compositions in the  $LS$ -coupling scheme. The average purities in the upper configuration were found to be 68% and 67% in  $LS$  and  $jj$  schemes, respectively. Note also that there is considerable term mixing, which leads to some ambiguity in term labels. The term labeled  $(^1D) ^2F_{5/2}$  has in fact a larger  $(^3P) ^2D_{5/2}$  component. However, the term with the largest  $(^3P) ^2D_{5/2}$  component has been given this designation. Similarly, the  $(^3P) ^2F_{7/2}$  term has a lower

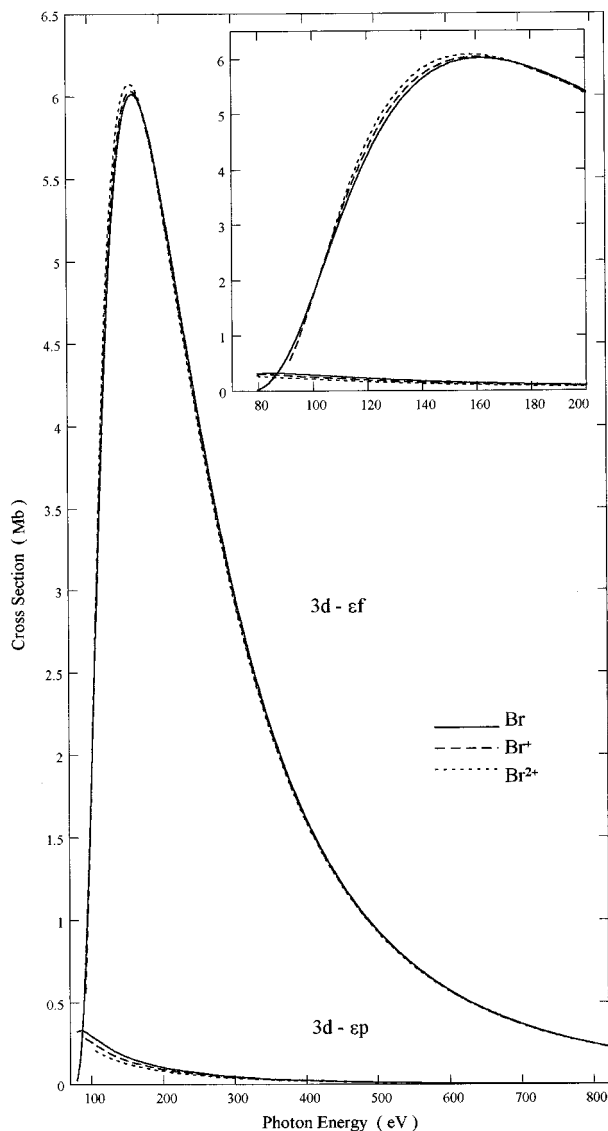


FIG. 12. Continuum cross sections for  $3d \rightarrow \epsilon p, \epsilon f$  photoionization in Br, Br<sup>+</sup>, and Br<sup>2+</sup>.

(<sup>3</sup>P) <sup>2</sup>F percentage (29%) than (<sup>3</sup>P) <sup>4</sup>D (38%), while the (<sup>1</sup>D) <sup>2</sup>F<sub>7/2</sub> term is 41% (<sup>3</sup>P) <sup>2</sup>F<sub>7/2</sub> in character.

At higher energies some discrete structure was observed. It consisted of discrete features at 90.37, 90.88, 91.39, and 91.78 eV superimposed on a background of almost continuum absorption and further structure extending from 90.5 eV with broad but weak peaks at 95.6, 97.14, 97.71, and 98.44 eV. Calculations predict that the lower-energy group is

associated with  $3d \rightarrow 5p$  transitions, while the higher-energy group arises from  $3d \rightarrow 6p$  excitation. Furthermore, although many hundreds of lines contribute to the spectrum in the 90–92 eV region, the calculations show that only five features with  $gf > 0.01$  arising from ground state <sup>4</sup>S<sub>3/2</sub> excitation are predicted. These are (<sup>3</sup>S) <sup>4</sup>P<sub>5/2</sub>, <sup>4</sup>P<sub>3/2</sub>, <sup>4</sup>P<sub>1/2</sub>, <sup>4</sup>P<sub>5/2</sub>, and <sup>4</sup>D<sub>5/2</sub> states at 89.60, 90.16, 90.40, 90.57, and 90.67 eV. The observed feature at 91.39 is the most intense and most likely corresponds to a blend of the features predicted for 90.40 and 90.57 eV. Thus the strongest lines can be readily accounted for if we add 0.7–1 eV to the calculated values.

Finally,  $3d$  partial cross sections for Br, Br<sup>+</sup>, and Br<sup>2+</sup> were computed to see if the  $3d \rightarrow \epsilon f$  is altered with increasing ionization. The results are shown in Fig. 12. To construct this figure continuum  $\epsilon p$  and  $\epsilon f$  wave functions were first obtained, the  $\langle 3d | r | \epsilon l \rangle$  matrix elements evaluated, and the formula of Manson and Cooper [20] applied to calculate the  $3d \rightarrow \epsilon p, \epsilon f$  cross sections. The  $3d \rightarrow \epsilon p$  cross section decays hydrogenically, while the  $3d \rightarrow \epsilon f$  cross section exhibits a minimum at threshold. However, the  $3d$  ionization potential is increasing so the  $3d \rightarrow \epsilon f$  peak actually moves closer to threshold with increasing ionization. Because of the non-linearity of our spectral detection and lack of absolute intensity calibration it was not possible to extract continuum absorption profiles from densitometer traces of the spectra.

#### IV. CONCLUSION

Discrete structure due to  $3d \rightarrow 4p$  photoexcitation for Br, Br<sup>+</sup>, and Br<sup>2+</sup> has been recorded and the origin of all of the strongest features has been identified. In addition, the strongest  $3d \rightarrow 5p, 6p$ , etc., transitions have also been observed. Cross sections for ground- and excited-state photoabsorption have been calculated and the dominant decay pathways of the resonances identified and predicted to be by direct autoionization.

#### ACKNOWLEDGMENTS

This work was supported by the Irish Science and Technology agency FORBAIRT under research Grant No. SC-95-403. We received partial support from the European Union under Contract No. CHRX-CT-93-0361. Many of the calculations were performed on the CRAY Y/MP-EL computer at the Queen's University, Belfast. The assistance of Cormac McGuinness and Padraig Dunne at different stages of this work are gratefully acknowledged. A.C. would also like to acknowledge financial support from the Department of Education for Northern Ireland.

[1] G. O'Sullivan, C. McGuinness, J. T. Costello, E. T. Kennedy, and B. Weinmann, Phys. Rev. A **53**, 3211 (1996).  
 [2] C. McGuinness, G. O'Sullivan, P. K. Carroll, D. Audley, and M. W. D. Mansfield, Phys. Rev. A **51**, 2053 (1995).  
 [3] G. O'Sullivan, P. K. Carroll, J. Conway, P. Dunne, R. Faulkner, T. McCormack, C. McGuinness, P. van Kampen, and B. Weinmann, Opt. Eng. **33**, 3993 (1994).

[4] E. T. Kennedy, J. T. Costello, J. P. Mosnier, A. A. Cafolla, M. Collins, L. Kiernan, U. Köble, M. H. Sayyad, M. Shaw, B. F. Sonntag, and R. Barchewitz, Opt. Eng. **33**, 3984 (1994).  
 [5] J. L. Tech, J. Res. Natl. Bur. Stand. A **67**, 505 (1963).  
 [6] R. E. Huffman, J. C. Larrabee, and Y. Tanaka, J. Chem. Phys. **47**, 856 (1967).  
 [7] V. N. Sarma, and Y. N. Joshi, J. Phys. B **16**, 1671 (1983).

- [8] B. Ruscic, J. P. Greene, and J. Berkowitz, *J. Phys. B* **17**, 1503 (1984).
- [9] D. M. de Leeuw, R. Mooyman, and C. A. de Lange, *Chem. Phys. Lett.* **54**, 236 (1978).
- [10] K. Kimura, T. Yamazaki, and Y. Achiba, *Chem. Phys. Lett.* **58**, 104 (1978).
- [11] S. T. Manson, A. Msezane, A. F. Starace, and S. Shahabi, *Phys. Rev. A* **20**, 1005 (1979).
- [12] F. Robicheaux and C. H. Greene, *Phys. Rev. A* **46**, 3821 (1992).
- [13] P. Van der Meulen, M. O. Krause, and C. A. de Lange, *J. Phys. B* **25**, 97 (1992).
- [14] F. Robicheaux and C. H. Greene, *Phys. Rev. A* **47**, 1066 (1993).
- [15] M. Mazzoni and M. Pettini, *Phys. Lett. A* **35**, 330 (1981).
- [16] L. Nahon, P. Morin, and F. Combet-Farnoux, *Phys. Scr.* **T41**, 104 (1992).
- [17] L. Nahon and P. Morin, *Phys. Rev. A* **45**, 2887 (1992).
- [18] R. D. Cowan, *The Theory of Atomic Structure and Spectra* (University of California Press, Berkeley, 1981).
- [19] R. L. Kelly, Oak Ridge National Laboratory Report No. 5922, 1982 (unpublished).
- [20] S. T. Manson and J. W. Cooper, *Phys. Rev.* **165**, 126 (1968).
- [21] E. J. McGuire, *Phys. Rev. A* **5**, 1052 (1972).
- [22] T. Hayashi, Y. Morioka, Y. Kageyama, M. Watanabe, I. H. Suzuki, A. Mikuni, G. Isoyama, S. Asaoka, and M. Nakamura, *J. Phys. B* **17**, 3571 (1984).
- [23] H. Aksela, S. Aksela, H. Pulkkinen, G. M. Bancroft, and K. H. Tan, *Phys. Rev. A* **33**, 3876 (1986).
- [24] U. Fano and J. W. Cooper, *Phys. Rev.* **137**, A1364 (1965).
- [25] G. C. King, M. Tronc, F. H. Read, and R. C. Bradford, *J. Phys. B* **10**, 2479 (1977).
- [26] F. Combet-Farnoux, *Phys. Scr.* **T41**, 28 (1992).
- [27] Y. N. Joshi, Th. A. M. van Kleef, and P. Uylings, *Phys. Lett.* **113A**, 479 (1985).